Received: 4 August 2020 | Revised: 3 September 2020 | Accepted: 19 October 2020

DOI: 10.1111/mpp.13017

ORIGINAL ARTICLE

Molecular Plant Pathology | WILEY

The conserved aromatic residue W^{122} is a determinant of potyviral coat protein stability, replication, and cell-to-cell movement in plants

Zhi-Yong Yan[1] | De-Jie Cheng[1] | Ling-Zhi Liu[1] | Chao Geng[1] | Yan-Ping Tian[1] | Xiang-Dong Li[1] | Jari P. T. Valkonen[2]

[1]Shandong Provincial Key Laboratory of Agricultural Microbiology, College of Plant Protection, Shandong Agricultural University, Tai'an, Shandong, China

[2]Department of Agricultural Sciences, University of Helsinki, Helsinki, Finland

Correspondence
Yan-Ping Tian and Xiang-Dong Li, Shandong Provincial Key Laboratory of Agricultural Microbiology, College of Plant Protection, Shandong Agricultural University, Tai'an, Shandong 271018, China.
Emails: yanping.tian@sdau.edu.cn (Y.-P. T.); xdongli@sdau.edu.cn (X.-D. L.)

Funding information
National Natural Science Foundation of China, Grant/Award Number: 31720103912

Abstract

Coat proteins (CPs) play critical roles in potyvirus cell-to-cell movement. However, the underlying mechanism controlling them remains unclear. Here, we show that substitutions of alanine, glutamic acid, or lysine for the conserved residue tryptophan at position 122 (W^{122}) in tobacco vein banding mosaic virus (TVBMV) CP abolished virus cell-to-cell movement in *Nicotiana benthamiana* plants. In agroinfiltrated *N. benthamiana* leaf patches, both the CP and RNA accumulation levels of three W^{122} mutant viruses were significantly reduced compared with those of wild-type TVBMV, and CP accumulated to a low level similar to that of a replication-deficient mutant. The results of polyprotein transient expression experiments indicated that CP instability was responsible for the significantly low CP accumulation levels of the three W^{122} mutant viruses. The substitution of W^{122} did not affect CP plasmodesmata localization or virus particle formation; however, the substitution significantly reduced the number of virus particles. The wild-type TVBMV CP could complement the reduced replication and abolished cell-to-cell movement of the mutant viruses. When the codon for W^{122} was mutated to that for a different aromatic residue, phenylalanine or tyrosine, the resultant mutant viruses moved systemically and accumulated up to 80% of the wild-type TVBMV level. Similar results were obtained for the corresponding amino acids of W^{122} in the watermelon mosaic virus and potato virus Y CPs. Therefore, we conclude that the aromatic ring in W^{122} in the core domain of the potyviral CP is critical for cell-to-cell movement through the effects on CP stability and viral replication.

KEYWORDS

cell-to-cell movement, coat protein, *Potyvirus*, replication, stability, *Tobacco vein banding mosaic virus*

1 | INTRODUCTION

The genus *Potyvirus*, belonging to the family *Potyviridae*, is the largest genus of plant RNA viruses, consisting of more than 160 species (Wylie et al., 2018). Many potyviruses cause severe economic losses in crop production (García et al., 2014; Scholthof et al., 2011; Valkonen, 2007). The potyvirus genome is a positive-sense single-stranded RNA molecule with 9,400 to 11,000 nucleotides.

The potyviral genomic RNA has a polyadenylated tail at its 3′ end and covalently links with a genome-linked protein (VPg) at its 5′ end (Tavert-Roudet et al., 2017; Wylie et al., 2018). The potyvirus genome encodes two polyproteins that are processed into 11 mature proteins by three self-encoded proteinases (Chung et al., 2008; Olspert et al., 2015; Revers & García, 2015; Rodamilans et al., 2015).

Cell-to-cell movement is a critical step for plant viruses to establish systemic infection (Ritzenthaler, 2011; Schoelz et al., 2011). To move between cells, plant viruses take advantage of plasmodesmata (PD), which are microscopic channels for plant communication between adjacent cells. Potyviruses do not encode a specific movement protein. However, the second 6 kDa protein (6K2) (Grangeon et al., 2013; Jiang et al., 2015), the third protein (P3) (Chai et al., 2020), the frame-shift protein P3N-PIPO produced by transcriptional slippage (Cheng et al., 2017; Geng et al., 2015; Olspert et al., 2015; Rodamilans et al., 2015; Wei et al., 2010), the cylindrical inclusion protein (CI) (Carrington et al., 1998; Deng et al., 2015; Movahed et al., 2017; Roberts et al., 1998; Rodríguez-Cerezo et al., 1997), and the coat protein (CP) (Dolja et al., 1994, 1995) are known to be involved in potyviral cell-to-cell movement.

Potyviral CPs contain three domains: the N-terminal domain with 17–78 residues (the numbers vary among viruses), the core domain with 213–218 residues (starting with the KDK/D residues at the N-terminus and ending with the TER/H residues at the C-terminus) (Shukla et al., 1988), and the C-terminal domain with 17–21 residues. Deletion of the N- or C- terminal domains of the tobacco etch virus (TEV) CP reduces its cell-to-cell movement in plants (Dolja et al., 1994, 1995). Alteration in the net charge of the N-terminal domain of the zucchini yellow mosaic virus CP, or mutation of the charged arginine residue at position 245 (R^{245}), histidine at position 246 (H^{246}), or aspartic acid at position 250 (D^{250}), which are at the border between the core and the C-terminal domains of the soybean mosaic virus CP, nearly abolishes viral cell-to-cell movement in plants (Kimalov, 2004; Seo et al., 2013). The phosphorylation sites in the T^{242}TSEED^{247} motif in CP are critical for the replication of potato virus A (Ivanov et al., 2003; Lõhmus et al., 2017). Mutation of the residues in serine (S^{122}), R^{154}, or D^{198} in the TEV CP completely abolishes TEV particle formation and cell-to-cell movement, suggesting that TEV moves between cells in the form of viral particles (Dolja et al., 1994, 1995). Although the core domain of the potyvirus CP is known to be involved in the viral cell-to-cell movement, the roles of the conserved amino acid residues in this domain in viral cell-to-cell movement remain largely unknown.

In this study, we determined that the aromatic ring of the conserved tryptophan residue at position 122 (W^{122}) in the potyvirus CP core domain plays an essential role in viral cell-to-cell movement through maintaining viral replication and CP stability.

2 | RESULTS

2.1 | Mutations of W^{122} abolish TVBMV cell-to-cell and systemic movement in *Nicotiana benthamiana* plants

To investigate the effects of conserved amino acid residues in the TVBMV CP on virus infection, we first aligned the CP sequences of 139 potyviruses and identified the completely conserved aromatic residue tryptophan (W) at position 122 (W^{122}; numbered according to the TVBMV CP sequence) (Figure S1). We then mutagenized the codon for W^{122} in the pCamTVBMV-GFP, an TVBMV infectious clone carrying the green fluorescent protein (GFP) gene, to the codons for residue alanine (A), glutamic acid (E), or lysine (K) to produce the plasmids pCamTVBMV^{W122A}-GFP, pCamTVBMV^{W122E}-GFP, and pCamTVBMV^{W122K}-GFP, respectively (Figure 1a). *Agrobacterium* cultures carrying pCamTVBMV-GFP or one of the three mutant plasmids were individually infiltrated into two expanded leaves of each assayed *N. benthamiana* plant to produce the viruses TVBMV-GFP, TVBMV^{W122A}-GFP, TVBMV^{W122E}-GFP, and TVBMV^{W122K}-GFP, respectively. At 7 days postagroinfiltration (dpai), the TVBMV-GFP-infected plants showed mosaic and epinasty symptoms in their systemically infected leaves, but the three mutant viruses did not (Figure 1b). When the infiltrated plants were examined under a UV light, the TVBMV-GFP-infected plants emitted a strong green fluorescence in their infiltrated and systemically infected leaves. This green fluorescence was only observed in the leaves infiltrated with pCamTVBMV^{W122A}-GFP, pCamTVBMV^{W122E}-GFP, and pCamTVBMV^{W122K}-GFP (Figure 1b). The results of the reverse transcription (RT)-PCR and western blot assays showed that TVBMV RNA and CP had accumulated in the systemically infected leaves of the TVBMV-GFP-inoculated plants, but not in the systemically infected leaves of the plants inoculated with one of the three mutant viruses (Figure 1c,d). To validate the importance of W^{122} in TVBMV systemic movement, we changed the codon of nonconserved residues arginine at position 62 (R^{62}) to that for A, cysteine (C), or E; serine at position 92 (S^{92}) to that for A, aspartic acid (D), or histidine (H); and K at position 246 (K^{246}) to that for A, C, or E in pCamTVBMV-GFP. These mutant plasmids were individually infiltrated into *N. benthamiana* leaves and these mutations did not inhibit viral systemic infection (Figure S2), indicating that W^{122} in the CP core domain was crucial for TVBMV systemic infection in *N. benthamiana* plants.

Next, we investigated the role of W^{122} in TVBMV cell-to-cell movement. *Agrobacterium* cultures carrying pCamTVBMV-GFP or one of its three W^{122} mutant plasmids were diluted to OD_{600} = 0.0001 and individually infiltrated into *N. benthamiana* leaves. GFP fluorescence from TVBMV-GFP was observed in clusters of multiple cells at 132 hr postagroinfiltration (hpai). However, the GFP fluorescence from TVBMV^{W122A}-GFP, TVBMV^{W122E}-GFP, or TVBMV^{W122K}-GFP was confined to single leaf cells (Figure 1e,f), indicating that W^{122} was also crucial for TVBMV cell-to-cell movement.

2.2 | Mutations of W^{122} inhibit TVBMV replication

Cell-to-cell movement and replication are two important and interconnected steps during potyvirus infection (Chai et al., 2020; Cui & Wang, 2016). To determine whether W^{122} has a role in TVBMV replication, we infiltrated *N. benthamiana* leaves with pCamTVBMV-GFP or one of the three W^{122} mutant plasmids. Plants infiltrated

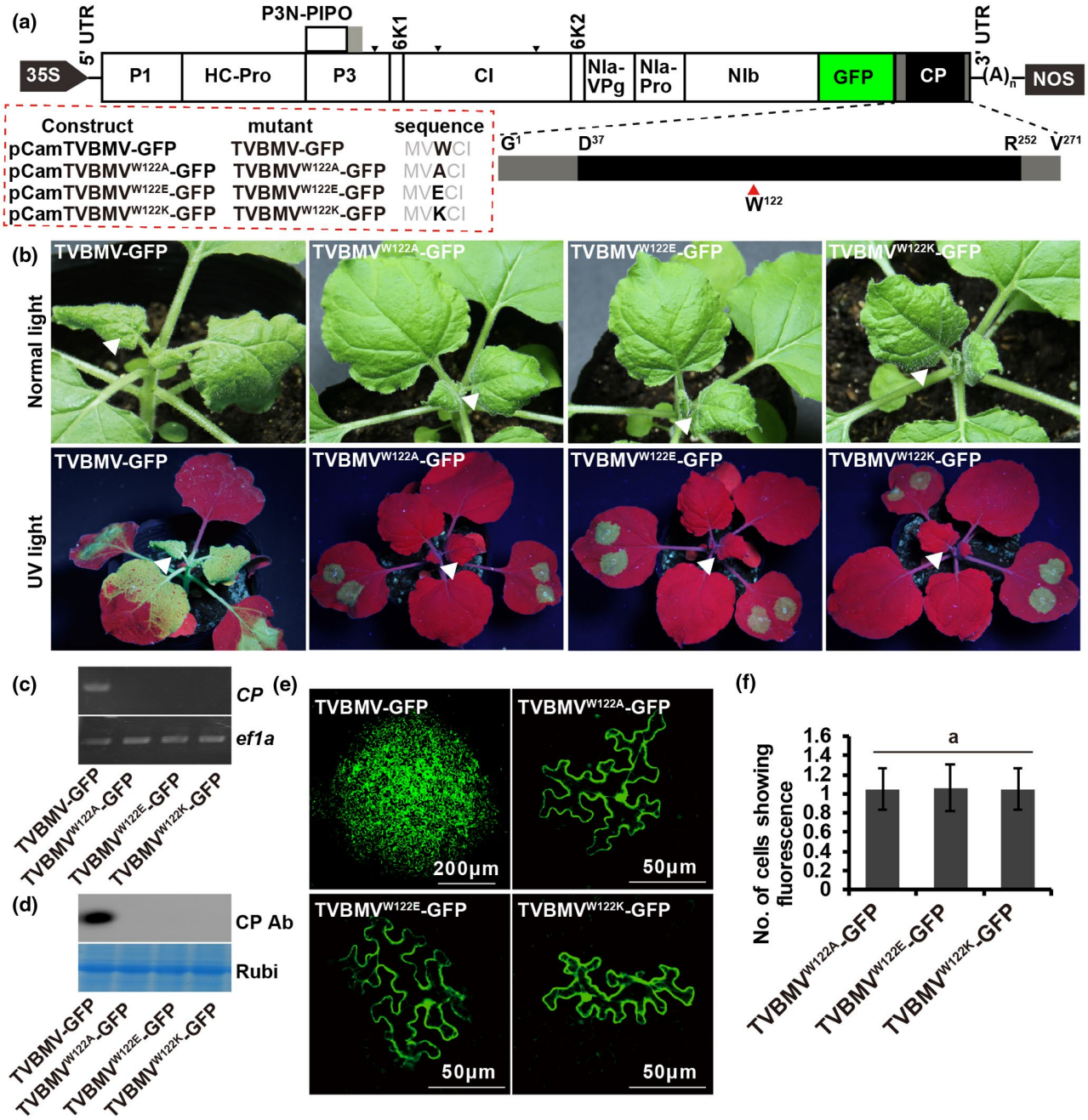

FIGURE 1 Conserved residue W^{122} in tobacco vein banding mosaic virus coat protein (TVBMV CP) is crucial for viral cell-to-cell and systemic movement. (a) A schematic diagram showing the genome organization of TVBMV in pCamTVBMV-GFP. The N- and C-terminal domains of TVBMV CP are in grey, and the core domain is in black. The relative position of W^{122} is indicated with a red arrowhead. The site-directed mutagenized plasmids (left column) and viruses (right column) are shown in the red-lined box. pCamTVBMV-GFP, pCamTVBMV^{W122A}-GFP, pCamTVBMV^{W122E}-GFP, and pCamTVBMV^{W122K}-GFP plasmids were individually agroinfiltrated into *Nicotiana benthamiana* plants. (b) Symptoms (upper panel) and green fluorescent protein (GFP) green fluorescence (lower panel) in various assayed *N. benthamiana* plants at 7 days postagroinfiltration (dpai) are shown. (c) and (d) Accumulation levels of TVBMV RNA and CP in the systemic leaves of the assayed plants were determined at 7 dpai through reverse transcription-PCR and western blot assay, respectively. The expression of the *Nbef1a* gene was used as an internal control during RT-PCR. Ab: antibody. The Coomassie brilliant blue-stained RuBisCO large subunit protein (Rubi) was used to show sample loadings. (e) and (f) Cell-to-cell movement of TVBMV-GFP and its three W^{122} mutants in *N. benthamiana* leaves at 132 hr postagroinfiltration (hpai). The pictures were taken under a confocal microscope at 132 hpai. Because each TVBMV-GFP infection focus contained too many cells with GFP fluorescence, its number is not shown in (f). The values are presented as means ± *SD* from 30 infection foci per treatment. Statistical significance between treatments was determined using Duncan's multiple range test ($p < .05$)

with pCamTVBMV^{NIbΔGDD}-GFP (produce replication-deficient mutant TVBMV^{NIbΔGDD}-GFP; Geng et al., 2017) or pCamTVBMV^{CPSTOP}-GFP (producing TVBMV^{CPSTOP}-GFP that did not produce CP) were used as controls. The infiltrated leaves were harvested at 60 hpai and analysed for GFP or CP accumulation using enzyme-linked immunosorbent assay (ELISA). The results showed that the accumulation levels of GFP in the TVBMV^{W122A}-GFP-, TVBMV^{W122E}-GFP-, or TVBMV^{W122K}-GFP-inoculated leaves were significantly reduced compared with that of the TVBMV-GFP-inoculated leaves. The accumulation levels of GFP in the TVBMV^{NIbΔGDD}-GFP- or TVBMV^{CPSTOP}-GFP-inoculated leaves were the lowest (Figure 2a). The accumulation levels of CP in the TVBMV^{W122A}-GFP-, TVBMV^{W122E}-GFP-, and TVBMV^{W122K}-GFP-inoculated leaf tissues were also significantly reduced compared with that of the TVBMV-GFP-inoculated leaf tissues and reached a similar level to that of mutant TVBMV^{NIbΔGDD}-GFP-inoculated leaf tissues (Figure 2b). Similar results were obtained using the leaf samples harvested at 108 hpai (Figure S3).

The accumulation levels of the TVBMV plus-strand (+)RNA and minus-strand (−)RNA in the infiltrated leaf tissues were determined using RT-quantitative PCR (RT-qPCR). The results showed that the accumulation levels of (+)RNA and (−)RNA in the TVBMV^{W122A}-GFP-, TVBMV^{W122E}-GFP-, or TVBMV^{W122K}-GFP-inoculated leaf tissues were significantly lower than that in the TVBMV-GFP-inoculated leaf tissues, but higher than those in the TVBMV^{NIbΔGDD}-GFP- or the TVBMV^{CPSTOP}-GFP-inoculated leaf tissues (Figure 2c,d), indicating that W^{122} in the CP could also affect TVBMV replication.

2.3 | W^{122} is crucial for TVBMV CP stability

To investigate why the three W^{122} mutants accumulated significantly less CP than TVBMV-GFP, we constructed two vectors to transiently express polyprotein, NIaPro:HA-NIb:GFP:CP and NIaPro:HA-NIb:GFP:CP^{W122A}, in *N. benthamiana* leaves through agroinfiltration (Figure 3a). Each of the polyproteins could be self-cleaved by NIaPro into four mature proteins: NIaPro, HA-NIb, GFP, and CP (or the mutant CP^{W122A}). *N. benthamiana* leaves were infiltrated with mixed *Agrobacterium* cultures harbouring pCamNIaPro:HA-NIb:GFP:CP and pBinP19, or pCamNIaPro:HA-NIb:GFP:CP^{W122A} and pBinP19. By 4 dpai, and the intensity of GFP fluorescence in the pCamNIaPro:HA-NIb:GFP:CP^{W122A} and pBinP19 coinfiltrated *N. benthamiana* leaf patches was similar to that in the pCamNIaPro:HA-NIb:GFP:CP and pBinP19 coinfiltrated leaf patches (Figure 3b). Western blot results showed that the accumulation levels of HA-NIb and GFP in the pCamNIaPro:HA-NIb:GFP:CP^{W122A} and pBinP19 coinfiltrated leaf patches were similar to those in the pCamNIaPro:HA-NIb:GFP:CP and pBinP19 coinfiltrated leaf patches (Figure 3c). However, the accumulation level of CP in the pCamNIaPro:HA-NIb:GFP:CP^{W122A} and pBinP19 coinfiltrated leaf patches was only one-ninth of that in the pCamNIaPro:HA-NIb:GFP:CP and pBinP19 coinfiltrated leaf patches (Figure 3c). These results suggest that mutation of W^{122} affects CP stability.

To further investigate the stability of the W^{122} mutant CP, we constructed pCamGFP-TVBMVCP and pCamGFP-TVBMVCP^{W122A} to express a GFP-TVBMVCP fusion and a GFP-TVBMVCP^{W122A} fusion, respectively (Figure 3d). *N. benthamiana* leaves were infiltrated with mixed *Agrobacterium* cultures harbouring pCamGFP-TVBMVCP and pBinP19, or pCamGFP-TVBMVCP^{W122A} and pBinP19. The infiltrated leaves were photographed and analysed at different times. The results showed that the intensity of GFP fluorescence in the leaf patches coexpressing GFP-TVBMVCP and P19 continued to increase from 30 to 120 hpai, whereas the intensity of GFP fluorescence in the leaf patches coexpressing GFP-TVBMVCP^{W122A} and P19 remained low (Figure 3e,f). We also constructed plasmids pCamTVBMVCP^{WT}

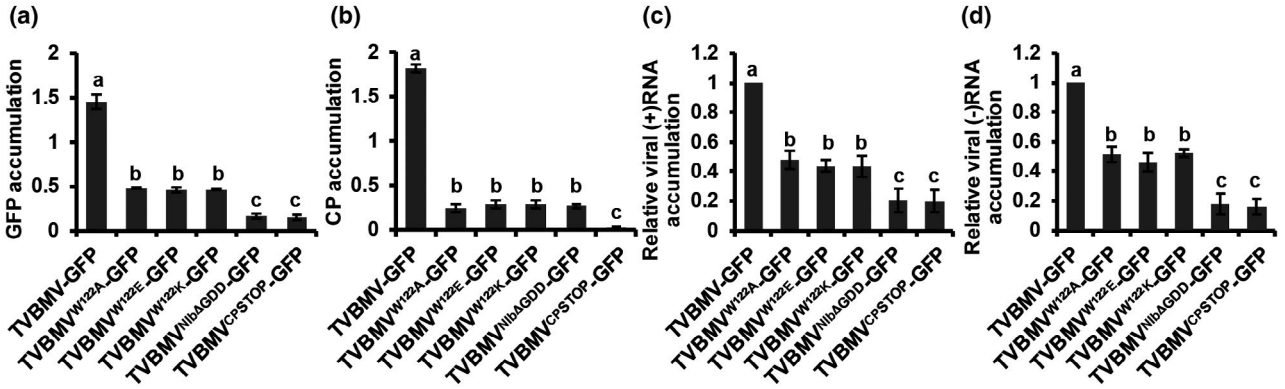

FIGURE 2 Conserved residue W^{122} in tobacco vein banding mosaic virus coat protein (TVBMV CP) is crucial for viral replication. The effect of W^{122} on TVBMV replication was tested by agroinfiltration of pCamTVBMV-GFP, pCamTVBMV^{W122A}-GFP, pCamTVBMV^{W122E}-GFP, pCamTVBMV^{W122K}-GFP, pCamTVBMV^{NIbΔGDD}-GFP, and pCamTVBMV^{CPSTOP}-GFP individually into *Nicotiana benthamiana* leaves. (a) and (b) The accumulation of green fluorescent protein (GFP) and TVBMV CP in various infiltrated leaf samples was determined through ELISA at 60 hr postagroinfiltration (hpai). The replication-deficient TVBMV^{NIbΔGDD}-GFP and TVBMV^{CPSTOP}-GFP mutants were included as controls. (c) and (d) The accumulation of TVBMV (+)RNA and (−)RNA in various infiltrated leaf samples was determined through quantitative reverse transcription PCR using specific primers at 60 hpai. The expression of *Nbef1a* was used as an internal control. The results are presented as means ± *SD* from three biological replicates per treatment. Statistical significance between treatments was determined using Duncan's multiple range test ($p < .05$)

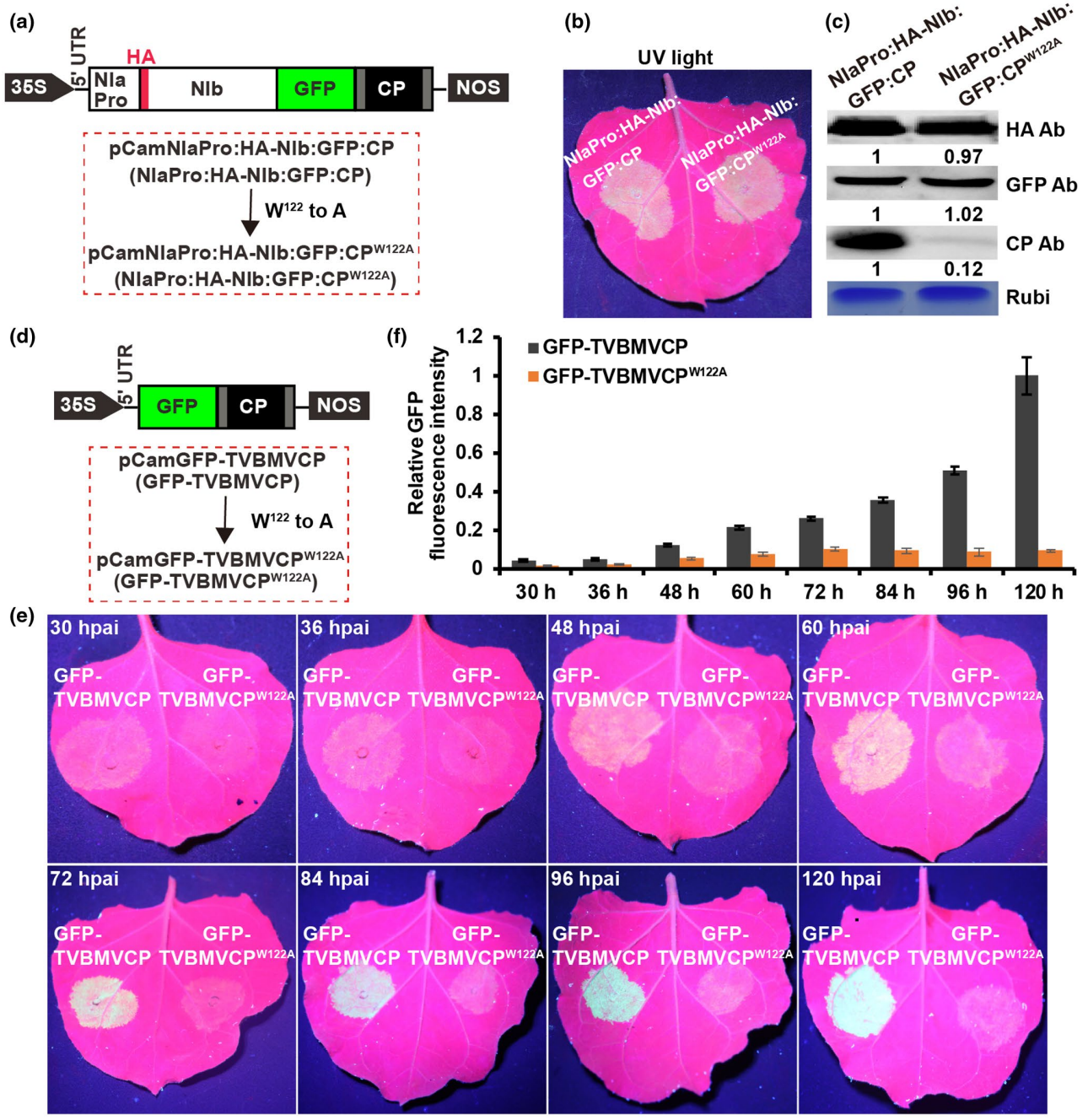

FIGURE 3 Effect of W^{122} on tobacco vein banding mosaic virus coat protein (TVBMV CP) stability. (a) A schematic diagram showing the NIaPro:HA-NIb:GFP:CP fragment in the pCamNIaPro:HA-NIb:GFP:CP vector. HA-NIb, GFP, and CP are cleaved from the polyprotein by NIaPro. (b) *Nicotiana benthamiana* leaves agroinfiltrated with pCamNIaPro:HA-NIb:GFP:CP and pBinP19 or pCamNIaPro:HA-NIb:GFP:CP^{W122A} and pBinP19 were photographed under a UV light at 4 days postagroinfiltration (dpai). (c) The accumulation of HA-NIb, green fluorescent protein (GFP), and CP in the infiltrated leaf patches was determined through western blot assay using a HA (upper panel), GFP (middle panel), or TVBMV CP (lower panel) specific antibody at 4 dpai. Ab, antibody. The Coomassie brilliant blue-stained RuBisCO large subunit protein (Rubi) was used to show sample loadings. (d) A schematic diagram showing plasmids expressing a GFP-TVBMVCP or GFP-$TVBMVCP^{W122A}$ mutant fusion. (e) A time-course study of GFP-TVBMVCP and GFP-$TVBMVCP^{W122A}$ expression in the infiltrated leaf patches at 30, 36, 48, 60, 72, 84, 96, and 120 hpai. (f) Analysis of GFP intensity in the pCamGFP-TVBMVCP and pCamGFP-$TVBMVCP^{W122A}$-infiltrated leaf patches at different time points using a microplate reader set at 485/10 nm (excitation wavelength) and 535/10 nm (emission wavelength). The values are presented as means ± *SD* from three biological replicates per treatment

and pCamTVBMVCP^{W122A} to transiently express TVBMVCP^{WT} and TVBMVCPW^{122A} in *N. benthamiana* leaves. Western blot results showed that, at 4 dpai, the accumulation levels of TVBMVCP^{WT} and TVBMVCP^{W122A} in the assayed leaf patches agreed with the results for GFP shown in Figure 3e,f (Figure S4). The expression of His-TVBMVCP and His-TVBMVCP^{W122A} in *Escherichia coli* cells also

indicated that the mutation of W^{122} to A affected the stability of TVBMV CP (Figure S5). All these results indicate that mutation of W^{122} affects CP stability.

2.4 | The mutation of W^{122} does not affect TVBMV particle formation

Previous studies have shown that virus particle formation is vital during potyviral cell-to-cell movement (Dolja et al., 1994). To determine whether the mutation of W^{122} could affect virus particle formation, we expressed TVBMV-GFP, TVBMV^{W122A}-GFP, TVBMV^{W122E}-GFP, and TVBMV^{W122K}-GFP in *N. benthamiana* leaves. At 5 dpai, the infiltrated leaves were collected and used for virus particle purification. When the purified samples were negatively stained with 2% uranyl acetate and examined under a transmission electron microscope, virus particles similar to that of TVBMV-GFP were observed in the TVBMV^{W122A}-GFP, TVBMV^{W122E}-GFP, and TVBMV^{W122K}-GFP purified samples, indicating that the mutation of W^{122} did not change the ability of CP to encapsidate viral RNA (Figure 4a). However, the numbers of virus particles in the TVBMV^{W122A}-GFP, TVBMV^{W122E}-GFP, and TVBMV^{W122K}-GFP purification samples were significantly reduced compared with that in the TVBMV-GFP purification sample (Figure 4b).

2.5 | The mutation of W^{122} does not affect the ability of CP to target PD

Potyviral CP, P3N-PIPO, and CI are known to target PD in cell walls and are necessary for the potyviral cell-to-cell movement (Wei et al., 2010). To investigate the effects of W^{122} on TVBMV CP subcellular localization, we coinfiltrated *N. benthamiana* leaves with mixed *Agrobacterium* cultures harbouring combinations of four constructs, including pCamTVBMV, pCamP3N-PIPO, pCamCI-DsRed, and pCamGFP-TVBMVCP or pCamGFP-TVBMVCP^{W122A}. At 48 hpai, analyses of infiltrated leaf patches under a confocal microscope showed that GFP-TVBMVCP and GFP-TVBMVCP^{W122A} could colocalize with CI-DsRed in the cell periphery targeted to PD (Figure 5). Our previous results showed that TVBMV CI can localize at PD in the presence of TVBMV P3N-PIPO (Geng et al., 2015). These results suggest that GFP-TVBMVCP and GFP-TVBMVCP^{W122A} could target PD with CI-DsRed and P3N-PIPO during TVBMV infection.

2.6 | Wild-type CP, but not the W122A mutant CP, rescue TVBMV^{W122A}-GFP replication and cell-to-cell movement

To determine whether TVBMVCP^{WT} (wild-type) or TVBMVCP^{W122A} could rescue the defective cell-to-cell movement of TVBMV^{W122A}-GFP, we infiltrated *N. benthamiana* leaves with a mixture of three *Agrobacterium* cultures harbouring pCamTVBMV^{W122A}-GFP, pCamTVBMVCP^{WT}, or pCamTVBMVCP^{W122A}, and pBinP19. The results showed

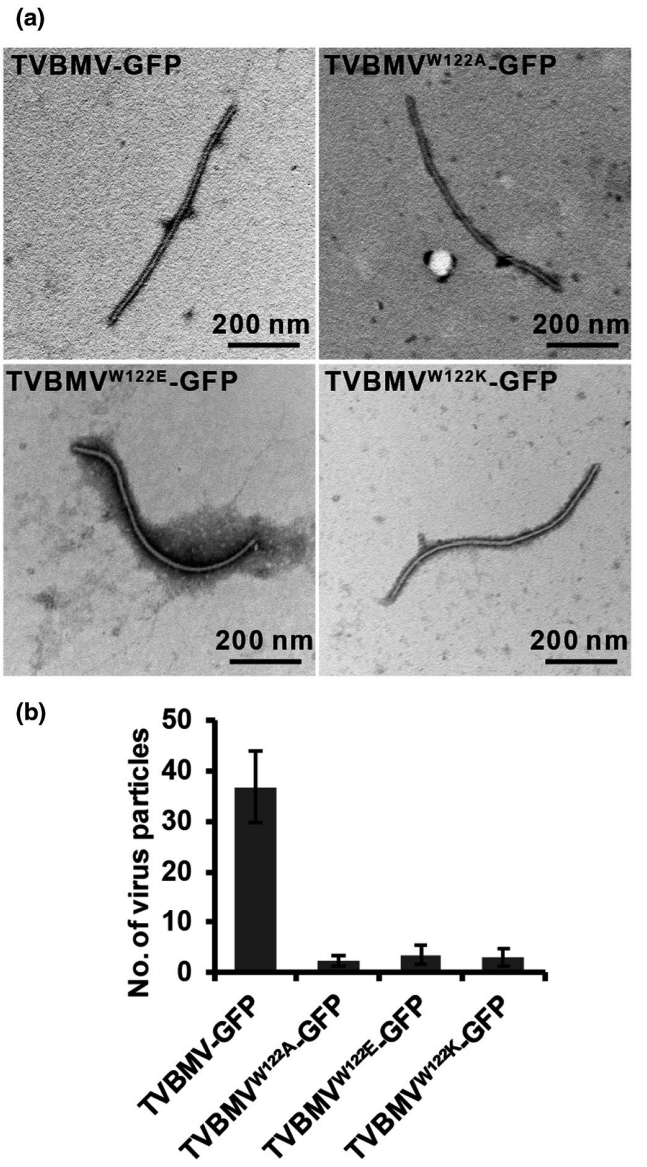

FIGURE 4 Effect of W^{122} on TVBMV particle formation. (a) Particles of TVBMV-GFP, TVBMV^{W122A}-GFP, TVBMV^{W122E}-GFP, and TVBMV^{W122K}-GFP. The virus particles were purified from the infiltrated leaf tissues, negatively stained with 2% uranyl acetate, and then examined under a transmission electron microscope. (b) The total numbers of virus particles in fields of 70 μm^2 were counted for each treatment and are presented as the means of virus particles per field ± *SD* from six fields per treatment

that, by 132 hpai, *N. benthamiana* leaves coexpressing TVBMV^{W122A}-GFP, TVBMVCP^{WT}, and P19 showed GFP fluorescence in multiple cells, indicating that TVBMVCP^{WT} rescued the cell-to-cell movement of TVBMV^{W122A}-GFP (Figure 6a,b). In contrast, the *N. benthamiana* leaves coexpressing TVBMV^{W122A}-GFP, TVBMVCP^{W122A}, and P19 showed GFP fluorescence in single cells only, indicating that TVBMVCP^{W122A} could not rescue the cell-to-cell movement of TVBMV^{W122A}-GFP.

To determine whether TVBMVCP^{WT} and TVBMVCP^{W122A} could rescue the replication of TVBMV^{W122A}-GFP, we infiltrated *N. benthamiana* leaves with a mixture of *Agrobacterium* cultures harbouring pCamTVBMV^{W122A}-GFP, pCamTVBMVCP^{WT}, or

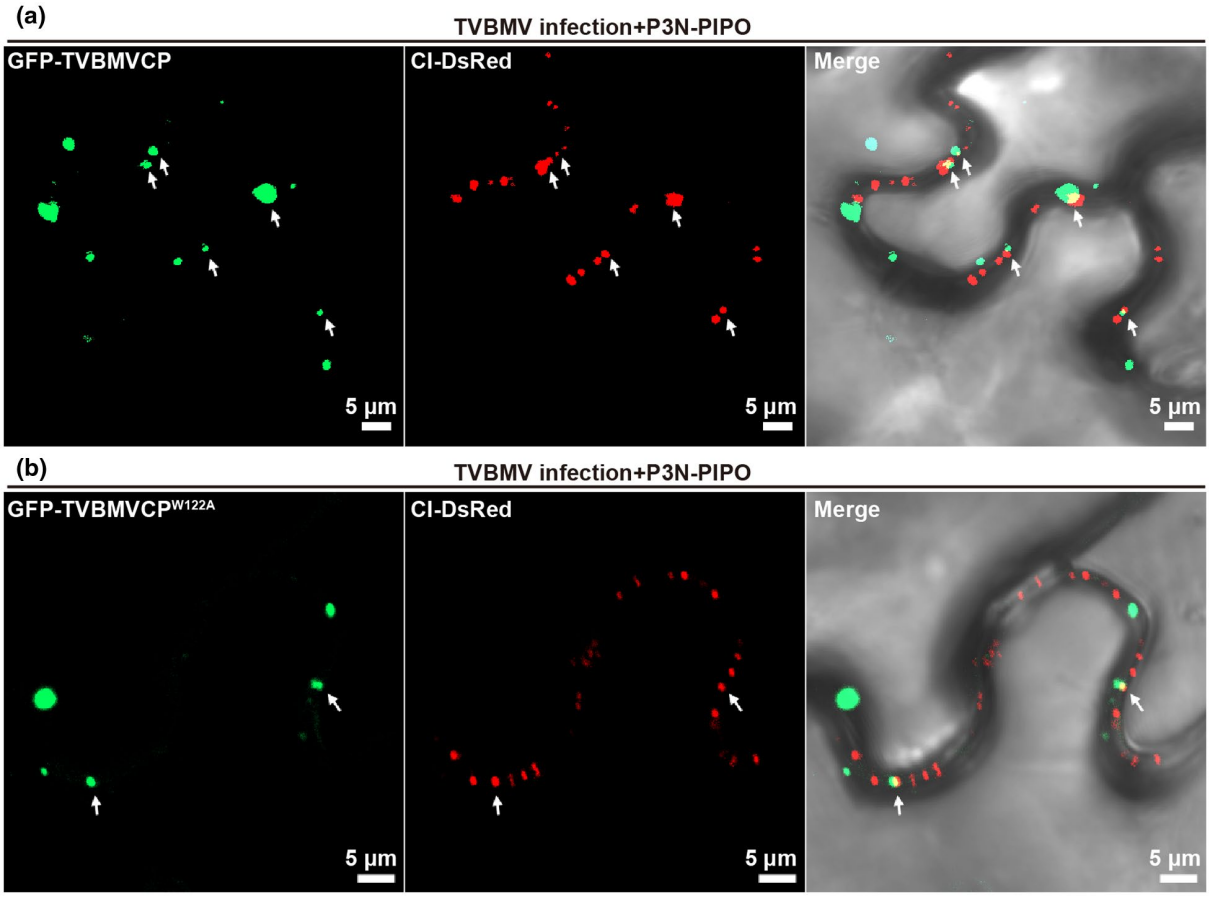

FIGURE 5 Effect of W^{122} on CP subcellular localization. In this experiment, we coinfiltrated *Nicotiana benthamiana* leaves with mixed *Agrobacterium* cultures harbouring various combinations of constructs: (a) pCamGFP-TVBMVCP, pCamTVBMV, pCamP3N-PIPO, and pCamCI-DsRed; (b) pCamGFP-TVBMVCP^{W122A}, pCamTVBMV, pCamP3N-PIPO, and pCamCI-DsRed. The infiltrated leaf tissues were collected at 48 hr postagroinfiltration (hpai) and examined under a confocal microscope. Both GFP-TVBMVCP and GFP-TVBMVCP^{W122A} were colocalized with CI-DsRed at the periphery of *N. benthamiana* leaf cells in the presence of TVBMV P3N-PIPO and TVBMV infection. White arrows indicate the points with both GFP-TVBMVCP and CI-DsRed or GFP-TVBMVCP^{W122A} and CI-DsRed. Bars = 5 μm. Pictures were photographed at 60 hpai under a confocal microscope

pCamTVBMVCP^{W122A}, and pBinP19, and analysed the harvested tissue samples through RT-qPCR at 60 hpai. The accumulation level of TVBMV^{W122A}-GFP (–)RNA in the leaf tissues coexpressing TVBMVCP^{WT} was partially rescued, whereas the accumulation level of TVBMV^{W122A}-GFP (–)RNA in the leaf tissues coexpressing TVBMVCP^{W122A} was not changed (Figure 6c), indicating that TVBMVCP^{WT} could rescue the replication of TVBMV^{W122A}-GFP.

We further found that TVBMVCP^{WT} and TVBMVCP^{W122A} could not rescue the replication and cell-to-cell movement of the replication-deficient mutant TVBMV^{CPSTOP}-GFP (Figure 6), suggesting that efficient viral replication is essential for TVBMV cell-to-cell movement.

2.7 | The aromatic ring of W^{122} is crucial for CP stability, TVBMV replication, and movement

Several studies have shown that aromatic residues in proteins play essential roles in protein stability and function (Budyak et al., 2013; Butterfield et al., 2002; Chatterjee et al., 2019; Rege et al., 2018). To determine whether the aromatic ring of the residue W^{122} was responsible for TVBMV cell-to-cell movement and CP stability, we mutated the codon for residue W^{122} in pCamTVBMV-GFP to the codons for the aromatic residue phenylalanine (F) or tyrosine (Y) to produce pCamTVBMV^{W122F}-GFP (TVBMV^{W122F}-GFP) and pCamTVBMV^{W122Y}-GFP (TVBMV^{W122Y}-GFP), and then individually infiltrated them into *N. benthamiana* leaves. By 7 dpai, both mutants TVBMV^{W122F}-GFP and TVBMV^{W122Y}-GFP caused systemic infection in *N. benthamiana*, although the GFP fluorescence from these two mutants was weaker than that of TVBMV-GFP under a UV light (Figure 7a). Western blot results revealed that the two mutants' CP accumulated approximately 82% and 77%, respectively, of the TVBMV-GFP CP level (Figure 7b). Analysis using RT-qPCR showed that, at 60 hpai, the accumulation levels of viral RNA in the systemic leaves and (–)RNA in the TVBMV^{W122F}-GFP and TVBMV^{W122Y}-GFP-inoculated *N. benthamiana* leaf patches were approximately 60% of the TVBMV-GFP level (Figure 7c,d).

We then mutated the W^{122} codon in pCamGFP-TVBMVCP to produce pCamGFP-TVBMVCP^{W122F} (GFP-TVBMVCP^{W122F}) and

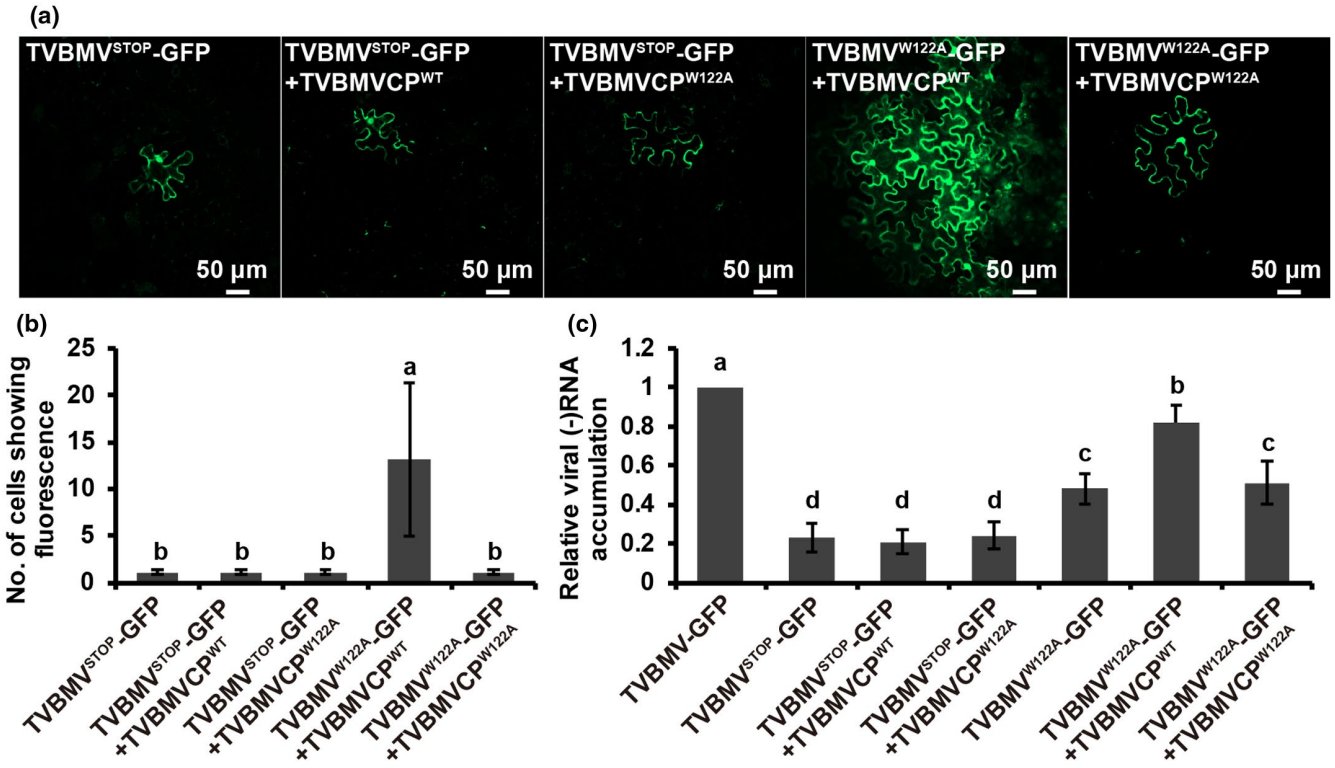

FIGURE 6 Wild-type (WT) CP could rescue the defective cell-to-cell movement and reduced replication of TVBMV^{W122}-GFP *in trans*. (a) Analysis of *trans*-complemented cell-to-cell movement by a movement-defective TVBMV^{W122A}-GFP. *Nicotiana benthamiana* leaves were coinfiltrated with a mixture of three *Agrobacterium* cultures carrying pCamTVBMV^{W122A}-GFP or pCamTVBMV^{CPSTOP}-GFP, pCamTVBMVCP^{WT} or pCamTVBMVCP^{W122A}, and pBinP19. The OD_{600} values were adjusted to 0.0003 for cultures carrying plasmids pCamTVBMV^{W122A}-GFP or pCamTVBMV^{CPSTOP}-GFP, and 0.6 for other plasmids before mixing. The infiltrated leaf tissues were harvested at 132 hr postagroinfiltration (hpai) and examined under a confocal microscope. Movement- and replication-defective mutant TVBMV^{CPSTOP}-GFP was included in the experiment as a control. Bars = 50 μm. (b) The numbers of cells with GFP fluorescence per infection foci per treatment at 132 hpai. The values are means ± *SD* from 30 infection foci per treatment. (c) The relative accumulation levels of TVBMV (−)RNA in the agroinfiltrated *N. benthamiana* leaf tissues at 60 hpai. *N. benthamiana* leaves were infiltrated with a mixture of three *Agrobacterium* cultures carrying pCamTVBMV^{W122A}-GFP or pCamTVBMV^{CPSTOP}-GFP, pCamTVBMVCP^{WT} or pCamTVBMVCP^{W122A}, and pBinP19. The OD_{600} value of cultures carrying any plasmid was 0.6 before mixing. The expression of *Nbef1a* was used as an internal control. The TVBMV-GFP (−)RNA accumulation was defined as 1. The results are presented as means ± *SD* from three biological replicates per treatment. Statistical significance between treatments was determined using Duncan's multiple range test ($p < .05$)

pCamGFP-TVBMVCP^{W122Y} (GFP-TVBMVCP^{W122Y}), and individually infiltrated them into *N. benthamiana* leaves. At 4 dpai, the GFP fluorescence intensity from GFP-TVBMVCP^{W122F} and GFP-TVBMVCP^{W122Y} reached approximately 60% of GFP-TVBMVCP, whereas that from GFP-TVBMVCP^{W122A} was only 17% (Figure 7e,f). When the codon for residue A in pCamGFP-TVBMVCP^{W122A} was changed back to the codon for residue W, the reverted mutant GFP-TVBMVCP$^{W122A\text{-}W}$ produced similar GFP fluorescence as GFP-TVBMVCP (Figure S6a,b). In this study, we also mutated the codon for W^{122} in pCamGFP-TVBMVCP to codons for nonaromatic residues R, asparagine (N), D, C, E, glutamine (Q), glycine (G), H, isoleucine (I), leucine (L), K, methionine (M), proline (P), S, threonine (T), or valine (V). After the infiltration of these mutant constructs to *N. benthamiana* leaves, none of the mutant fusion proteins produced visible GFP fluorescence in the leaf patches (Figure S6a,b). When the above mutations were introduced into pCamTVBMV-GFP, all the mutant viruses were confined to single cells (Figure S6c). Deletion of the W^{122} codon from pCamGFP-TVBMVCP or pCamTVBMV-GFP reduced the accumulation level of the mutant GFP-TVBMVCP^{W122A} and abolished the cell-to-cell movement of TVBMV ^{W122del}-GFP (Figure S6).

2.8 | The corresponding residues of W^{122} in watermelon mosaic virus CP or potato virus Y CP are also critical for viral cell-to-cell movement and CP accumulation

W^{133} in watermelon mosaic virus (WMV) CP and residue W^{118} in potato virus Y (PVY) CP are the corresponding residues of W^{122} in TVBMV CP. To investigate whether W^{133} and W^{118} were also crucial for viral cell-to-cell movement, we deleted the codon for W^{133} in pCBWMV-GFP and the codon for W^{118} in pCamPVY-GFP to produce pCBWMV^{W133del}-GFP and pCamPVY^{W118del}-GFP, respectively. We then individually infiltrated pCBWMV-GFP, pCBWMV^{W133del}-GFP, pCamPVY-GFP, and pCamPVY^{W118del}-GFP into *N. benthamiana*

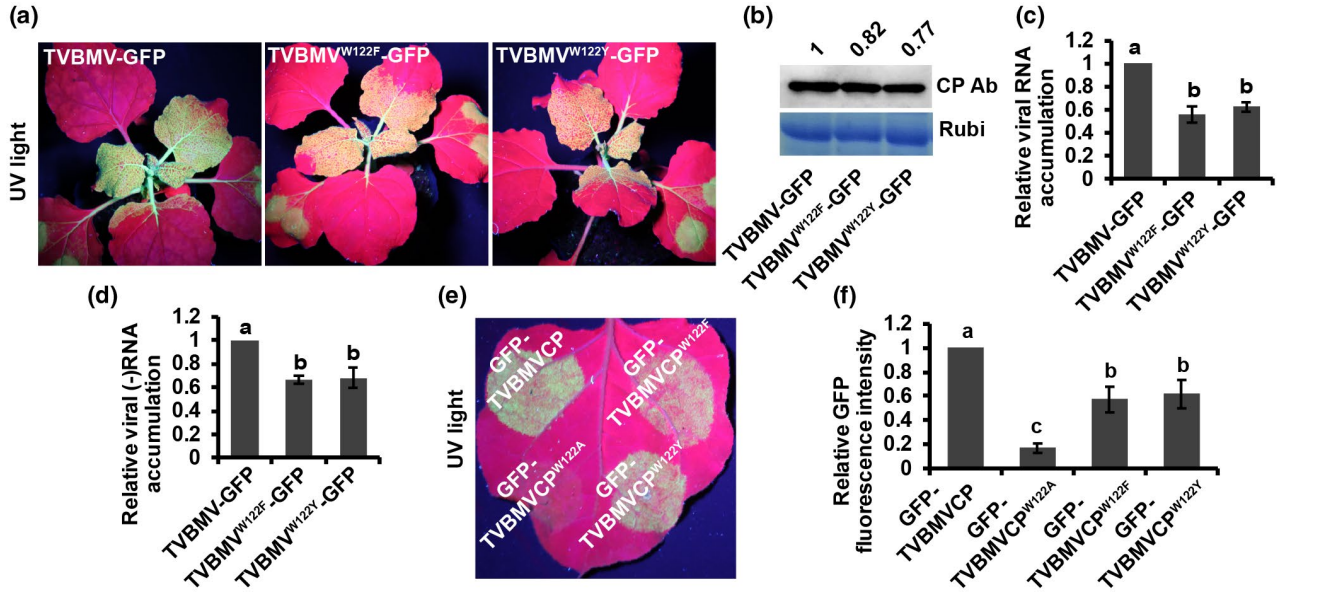

FIGURE 7 Effects of aromatic residues on TVBMV infection and CP stability. (a) GFP fluorescence in the systemic leaves of *Nicotiana benthamiana* plants infected with TVBMV-GFP, TVBMV^{W122F}-GFP, and TVBMV^{W122Y}-GFP at 7 days postagroinfiltration (dpai). The W^{122} codon in pCamTVBMV-GFP was mutated to the F or Y codons to produce pCamTVBMV^{W122F}-GFP and pCamTVBMV^{W122Y}-GFP, which were individually infiltrated into *N. benthamiana* leaves. (b) and (c) The accumulation levels of TVBMV CP and RNA in different leaf samples at 7 dpai. Accumulation of CP was determined through western blot assay using a TVBMV CP-specific antibody. Ab, antibody. Coomassie brilliant blue-stained RuBisCO large subunit protein (Rubi) was used to show sample loadings. The expression of *Nbef1a* was used as an internal control in quantitative reverse transcription PCR (RT-qPCR). (d) The accumulation levels of TVBMV (–)RNA in *N. benthamiana* leaf patches infiltrated with pCamTVBMV-GFP, pCamTVBMV^{W122F}-GFP, or pCamTVBMV^{W122Y}-GFP at 60 hpai were analysed using RT-qPCR. The expression of *Nbef1a* was used as an internal control in RT-qPCR. The results are presented as means ± *SD* from three biological replicates per treatment. (e) GFP fluorescence in *N. benthamiana* leaf patches agroinfiltrated with pCamGFP-TVBMVCP, pCamGFP-TVBMVCP^{W122A}, pCamGFP-TVBMVCP^{W122F}, and GFP-TVBMVCP^{W122Y}. The leaf was photographed under a UV light at 4 dpai. (f) Relative GFP fluorescence intensity in *N. benthamiana* leaf patches agroinfiltrated with pCamGFP-TVBMVCP, pCamGFP-TVBMVCP^{W122A}, pCamGFP-TVBMVCP^{W122F}, and GFP-TVBMVCP^{W122Y}. Analysis of GFP fluorescence intensity was conducted at 4 dpai using a microplate reader. The results are presented as means ± *SD* from three biological replicates per treatment. The statistical significance between treatments was determined using Duncan's multiple range test ($p < .05$)

leaves. At 132 hpai, GFP fluorescence was observed in clusters of multiple cells infected with WMV-GFP or PVY-GFP. In contrast, GFP fluorescence from WMV^{W133del}-GFP or PVY^{W118del}-GFP was confined to single cells (Figure 8a,b), indicating that residues W^{133} and W^{118} were also crucial for viral cell-to-cell movement.

To investigate the roles of W^{133} and W^{118} in viral CP accumulation, we constructed pCamGFP-WMVCP, pCamGFP-WMVCP-^{W133del}, pCamGFP-PVYCP, and pCamGFP-PVYCP^{W118del}, and then individually infiltrated them into *N. benthamiana* leaves. The results showed that, at 4 dpai, the GFP fluorescence from the two mutant proteins was significantly weaker than that from the two parental proteins (Figure 8c,d), indicating that residue W^{133} in WMV CP and residue W^{118} in PVY CP are crucial for CP accumulation.

3 | DISCUSSION

We studied the role of the conserved residue W^{122} in the TVBMV CP core domain in viral cell-to-cell movement and replication. Our results showed that mutation of W^{122} to various nonaromatic residues reduced viral replication and CP stability, leading to a defective viral cell-to-cell movement. Additionally, the aromatic ring of W^{122} was a key determinant of TVBMV CP stability, viral replication, and cell-to-cell movement.

CP is one of the potyviral proteins involved in viral cell-to-cell movement. It has been reported that a change in a single residue in the CP can affect potyviral cell-to-cell movement. For example, mutation of conserved residue S^{129}, R^{161}, or D^{205} (positions are numbered according to the TVBMV CP sequence) in the TEV CP core domain abolishes viral cell-to-cell movement (Dolja et al., 1994, 1995). In this study, the aromatic residue W^{122} in the CPs of 139 potyviruses was completely conserved (Figure S1). Mutation of W^{122} to various nonaromatic residues abolished TVBMV cell-to-cell movement (Figures 1e,f and S6c). Additionally, the deletion of W^{133} residue from WMV CP and the W^{118} residue from PVY CP abolished WMV and PVY cell-to-cell movement in *N. benthamiana* leaves (Figure 8a,b). Because W^{118} and W^{133} corresponded to W^{122} in TVBMV CP, we concluded that the conserved residue W^{122} was a key determinant of the potyviral cell-to-cell movement.

It is noteworthy that the three TEV movement-deficient mutants derived from S^{129}, R^{161}, and D^{205} do not produce virus particles (Dolja et al., 1994, 1995). The deletion of 65 residues from the C-terminus of

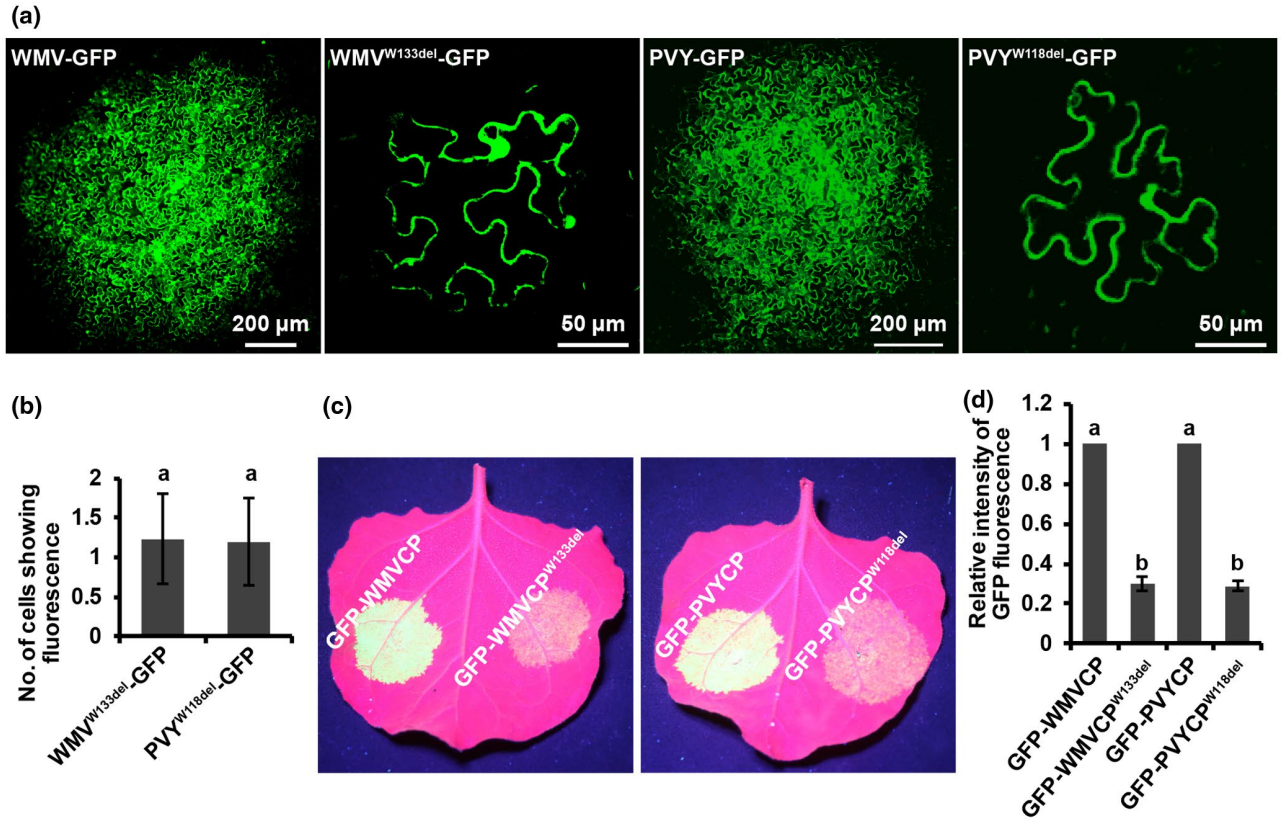

FIGURE 8 Deletion of W^{133} from watermelon mosaic virus coat protein (WMV CP) or W^{118} from potato virus Y (PVY) CP abolished viral cell-to-cell movement and reduced viral CP accumulation. (a) The cell-to-cell movement of WMV-GFP, $WMV^{W133del}$-GFP, PVY-GFP, and $PVY^{W118del}$-GFP in *Nicotiana benthamiana* plants at 132 hr postagroinfiltration. The infiltrated leaves were sampled, examined, and imaged under a confocal microscope. GFP fluorescence indicates a virus infection. (b) The numbers of cells with GFP fluorescence presented as the means ± *SD* from 30 infection foci per treatment. The infection foci caused by WMV-GFP or PVY-GFP infection had too many cells with GFP fluorescence and are not presented here. (c) GFP fluorescence in the leaf patches expressing GFP-WMVCP, GFP-$WMVCP^{W133del}$, GFP-PVYCP, or GFP-$PVYCP^{W118del}$. (d) GFP fluorescence intensity in different leaf patches expressing GFP-WMVCP, GFP-$WMVCP^{W133del}$, GFP-PVYCP, or GFP-$PVYCP^{W118del}$ as determined at 4 days postagroinfiltration using a microplate reader. The results are presented as means ± *SD* from three biological replicates per treatment. Statistical significance between treatments was determined using Duncan's multiple range test ($p < .05$)

wheat streak mosaic virus (*Tritimovirus*, family *Potyviridae*) CP inhibits viral cell-to-cell movement but has no apparent effect on virus particle formation (Tatineni et al., 2014). We found that mutations of W^{122} to A, E, or K did not change TVBMV particle morphology, but inhibited viral cell-to-cell movement (Figures 1 and 4). Wei et al. (2010) reported that in the presence of turnip mosaic virus (TuMV) P3N-PIPO or during TuMV infection, TuMV CP and CI can accumulate adjacent to PD, which is a necessary step during potyviral cell-to-cell movement. In this study, we discovered that TVBMV CP and CI also accumulated adjacent to the PD in the presence of P3N-PIPO and TVBMV infection. Furthermore, the ability of TVBMV CP to target PD was not affected by the change in W^{122} to A (Figure 5). Therefore, we concluded that the role of W^{122} was in viral cell-to-cell movement, but not in viral RNA encapsidation.

Previous studies have shown that potyviral replication and cell-to-cell movement are coupled processes (Chai et al., 2020; Cui & Wang, 2016). Here, we found that substitution of conserved W^{122} to nonaromatic residues significantly inhibited, but did not abolish, the replication of mutant viruses (Figure 2c,d). Interestingly, the CP accumulation levels of these W^{122} virus mutants were similar to that of the defective virus mutant $TVBMV^{NIb\Delta GDD}$-GFP (Figure 2b). The abolished cell-to-cell movement of $TVBMV^{W122A}$-GFP could be rescued by coexpressing $TVBMVCP^{WT}$ (Figure 6). In the same experiment, the RNA accumulation level of $TVBMV^{W122A}$-GFP was also increased. These results indicate that the reduced viral replication and extremely low CP accumulation might be both responsible for the defective cell-to-cell movement of W^{122} mutant viruses.

Potyviruses adopt a polyprotein expression strategy. The accumulation of individual viral proteins in the same tissues is assumed to be at the same level. The accumulating levels of (+)RNA and (−)RNA derived from W^{122} mutant viruses were much higher than those of the $TVBMV^{NIb\Delta GDD}$-GFP and $TVBMV^{CPSTOP}$-GFP mutant viruses (Figure 2c,d). The GFP accumulation levels of the three W^{122} mutant viruses were significantly higher than that of $TVBMV^{NIb\Delta GDD}$-GFP, but not the accumulation levels of their CPs (Figure 2a,b). We considered that the mutations introduced to W^{122} destabilized the CPs. This conclusion was supported because substitution of A for W^{122} in the polyprotein NIa:HA-NIb:GFP:CP did not change the accumulation levels of HA-NIb and GFP, but reduced the accumulation level of mutant CP (Figure 3c).

Ubiquitin signalling and autophagy are two critical pathways that control protein degradation (Goldberg, 2012; Olzmann et al., 2004, 2007). It has been reported that inhibition of proteasome activity using MG132 enhanced potato virus A CP accumulation (Lõhmus et al., 2017), indicating that ubiquitin signalling can regulate virus CP degradation. The conserved helix in the C-terminal region of the NSs protein of the watermelon silver mottle virus (WSMoV) is critical for protein stability. However, the accumulation of WSMoV with mutations in the conserved helix is not affected by MG132 treatment (Huang et al., 2020). In this study, treatment of leaves with MG-132 or 3-MA, a specific inhibitor of autophagy (Seglen & Gordon, 1982), had no significant effect on the accumulation of GFP-TVBMVCP or mutant GFP-TVBMVCP^{W122A} (Figure S7), suggesting that ubiquitin signalling and autophagy may not be the factors causing TVBMV CP instability.

The aromatic residues W, F, and Y are known to be important for protein stability and function. For example, the aromatic ring of Y^{398} in the WSMoV NSs protein has been shown to affect NSs stability and its RNA silencing suppression activity (Huang et al., 2015). Deletion of five residues, including an aromatic residue, from the readthrough protein of potato leafroll virus affects viral systemic infection and disease symptom induction (Xu et al., 2018). In this study, after mutation of W^{122} to nonaromatic residue A, E, or K, the mutant viruses produced destabilized CPs and exhibited reduced viral replication and defective viral cell-to-cell movement (Figures 1 and 2). Substitutions of other nonaromatic residues for W^{122} produced the same results (Figure S6). In contrast, changing residue W^{122} to aromatic residues F or Y yielded two mutant viruses capable of replicating to c.60% of TVBMV-GFP in the infiltrated leaves and c.80% of TVBMV CP in the systemically infected leaves (Figure 7d). Because similar results were obtained for WMV and PVY CPs (Figure 8), we concluded that the aromatic residue W^{122} was a determinant of potyviral CP stability, replication, and movement. Aromatic rings can interact with each other to stabilize proteins. In a recent report, aromatic ring interaction between Y^{51} and F^{64} in the small ubiquitin-like modifier (SUMO) is vital to SUMO stability and its SUMOylation activity (Chatterjee et al., 2019). We speculate that the aromatic ring of W^{122} also interacts with other residues to stabilize CP, leading to successful cell-to-cell movement.

The aromatic ring of residue W^{122} is a critical factor for potyviral replication and CP stability. As a result, mutation of W^{122} to a nonaromatic residue abolishes potyviral cell-to-cell movement. The findings presented here increase our understanding of the underlying mechanism controlling potyviral cell-to-cell movement. Further studies are necessary to elucidate the roles of CP secondary or higher structures during potyvirus infection in plants.

4 | EXPERIMENTAL PROCEDURES

4.1 | Amino acid sequence alignments

CP sequences of 139 potyviruses were downloaded from a reference sequence database at the National Center for Biotechnology Information (O'Leary et al., 2016). Multiple sequence alignments were performed using the ClustalW program in BioEdit v. 7.2.6, using the default parameters (Hall, 1999). The resulting FASTA file was further processed using the online application WebLogo (http://weblogo.berkeley.edu) to generate sequence logos as previously described (Crooks, 2004).

4.2 | Plasmid construction and site-directed mutagenesis

The *gfp* gene-containing infectious clones pCamTVBMV-GFP (accession number: JQ407082), pCBWMV-GFP, pCamPVY-GFP, and the infectious clone pCamTVBMV without *gfp* gene were constructed in our laboratory (Gao et al., 2012; Geng et al., 2015). The coding sequences of TVBMV CP, WMV CP, and PVY CP were PCR-amplified from the above infectious clones and individually inserted into the expression vector pCam35S::GFP to produce pCamGFP-TVBMVCP, pCamGFP-WMVCP, and pCamGFP-PVYCP, respectively. The TVBMV CI coding region was PCR-amplified and cloned into a different expression vector pCam35S::DsRed to produce pCamCI-DsRed. The coding regions of TVBMV P3N-PIPO, CP, and NIaPro:NIb:GFP:CP were PCR-amplified and cloned individually into the pCam35S vector to produce pCamTVBMV-VCP^{WT}, pCamP3N-PIPO, and pCamNIaPro:NIb:GFP:CP, respectively. An HA-tag encoding sequence was inserted between the first and second codons of the NIb open reading frame (ORF) in the pCamNIaPro:NIb:GFP:CP clone to produce pCamNIaPro:HA-NIb:GFP:CP. For expression of TVBMV CP in *E. coli* cells, the CP sequence was cloned into vector pEHISTEV to produce pEHISTEV-TVBMVCP. To generate a replication-deficient TVBMV mutant, we deleted the codons for the conserved GDD motif in the NIb ORF in pCamTVBMV-GFP to produce pCamTVBMV$^{NIb\Delta GDD}$-GFP as described (Geng et al., 2017). A stop codon was inserted immediately after the second codon in the CP ORF in pCamTVBMV-GFP to produce pCamTVBMV^{CPSTOP}-GFP. Substitutions of the codons for alanine (A), glutamic acid (E), or lysine (K) for that of W^{122} in pCamTVBMV-GFP were performed using site-directed mutagenesis as previously described (Liu & Naismith, 2008) to produce pCamTVBMV^{W122A}-GFP, pCamTVBMV^{W122E}-GFP, and pCamTVBMV^{W122K}-GFP, respectively. The codon for W^{133} in pCBWMV-GFP and the codon for W^{118} in pCamPVY-GFP were deleted to produce pCBWMV^{W133del}-GFP and pCamPVY^{W118del}-GFP, respectively. All plasmids were sequenced before use. Primers used in this study are listed in Table S1. The names and products of various constructs used in this study are listed in Table S2.

4.3 | Plant growth, virus inoculation, and protein transient expression

N. benthamiana plants were grown in a greenhouse set at 25 °C and a 16/8 hr (light/dark) photoperiod. Plasmids were individually

transformed into *Agrobacterium tumefaciens* GV3101 cells using a freeze-thaw method. *Agrobacterium* cultures harbouring different plasmids were cultured overnight in Luria–Bertani liquid medium supplemented with appropriate antibiotics at 28 °C with 220 rpm shaking. The cultures were pelleted through centrifugation at 8,000 × g for 2 min and individually resuspended in an induction buffer containing 10 mM $MgCl_2$, 10 mM MES, and 150 μM acetosyringone. To determine viral accumulation in the infiltrated leaf patches and systemic movement in the plants, the agrobacterium cultures were diluted to OD_{600} = 0.2. To determine viral cell-to-cell movement, the agrobacterium cultures were diluted to OD_{600} = 0.0001. For transient expression assays, individual agrobacterium cultures were diluted to OD_{600} = 0.4 and then mixed with an agrobacterium culture (1:1 vol/vol) harbouring pBinP19, a vector expressing tomato bushy stunt virus P19 protein. For cell-to-cell movement *trans*-complementation assays, the agrobacterium cultures carrying pCamTVBMV^{CPSTOP}-GFP or pCamTVBMV^{W122A}-GFP were diluted to OD_{600} = 0.0003 and the cultures carrying pCamTVBMVCP^{WT} or pCamTVBMVCP^{W122A} were diluted to OD_{600} = 0.6. These cultures were individually mixed with an equal volume of culture carrying pBinP19 (OD_{600} = 0.6). For viral replication *trans*-complementation assays, the agrobacterium cultures carrying pCamTVBMV^{CPSTOP}-GFP or pCamTVBMV^{W122A}-GFP, pCamTVBMVCP^{WT} or pCamTVBMVCP^{W122A}, and pBinP19 were diluted to OD_{600} = 0.6 and mixed at a ratio of 1:1:1. After 3 hr incubation at 25 °C, the cultures were individually infiltrated into leaves of 4–6-week-old *N. benthamiana* plants with 1-ml needleless syringes. The infiltrated plants were grown in a greenhouse till use. For protein degradation assays, a 1% dimethyl sulphoxide (DMSO) (control) solution or 50 μM MG132 (Selleck Chemicals) in 1% DMSO was infiltrated into *N. benthamiana* leaves to inhibit the ubiquitin signalling pathway. Water (control) or a 5 mM 3-methyladenine (3-MA) (Selleck Chemicals) aqueous solution was used to inhibit the autophagy pathway in leaves.

4.4 | RNA extraction and RT-qPCR

The infiltrated leaf tissues or the systemic leaves were collected from the assayed *N. benthamiana* plants and used for total RNA extraction using TransZol reagent (TransGen Biotech). The resulting total RNA samples were treated with a gDNA wipe enzyme (Vazyme) to remove plant genomic DNA. For RT-qPCR analysis of viral RNA accumulation, 500 ng total RNA (per sample) was reverse transcribed using a HiScript II Q RT SuperMix kit supplemented with random primers (Vazyme). To detect viral plus- and minus-strand RNA accumulation in the infiltrated leaf tissues, 500 ng total RNA (per sample) was reverse transcribed using primers qTVBMVCP-R and EF1A-R or primers qTVBMVCP-F and EF1A-R, and the HiScript II Q RT select SuperMix. Quantitative PCR was conducted using a ChamQ SYBR qPCR Master Mix (Vazyme) on a thermocycler (LC96; Roche). TVBMV *CP*-specific qPCR primers are listed in Table S1. The expression of *N. benthamiana ef1a* was determined using primer EF1A-F and EF1A-R, and was used as an internal control.

4.5 | Western blot assay

Systemically infected leaves or the infiltrated leaf tissues were collected from the assayed *N. benthamiana* plants and homogenized individually in a protein extraction buffer (100 mM Tris-HCl, 150 mM NaCl, 1 mM EDTA, 5% sucrose, and 1 mM phenylmethanesulfonyl fluoride) at a ratio of 1:2 (wt/vol) using a tissue grinder (Jingxin). The leaf extracts were denatured at 95 °C for 5 min, incubated on ice for 5 min, and then centrifuged at 12,000 × g for 5 min. The supernatant was collected from each sample, and the proteins in each sample were separated in SDS-polyacrylamide gels through electrophoresis and then blotted onto nitrocellulose membranes. Polyclonal antibodies specific for TVBMV CP or GFP were prepared in our laboratory (Ji et al., 2018; Lan et al., 2007) and were all used at a 1:1,000 (vol/vol) dilution. The HA-specific antibody (Thermo Fisher Scientific) was used at a 1:1,000 dilution. A horseradish peroxidase-conjugated goat anti-rabbit IgG (Sigma-Aldrich) was used as the secondary antibody diluted at 1:50,000 (vol/vol). After the addition of the SuperSignal West Dura extended duration substrate solution (Thermo Fisher Scientific), the detection signal was visualized using a chemiluminescent imaging and analysis system (Sage).

4.6 | ELISA

The collected plant tissues were individually homogenized (1:8, wt/wt) in a coating buffer (15 mM Na_2CO_3, 35 mM $NaHCO_3$, pH 9.6). Aliquots (100 μl) of leaf crude extracts were added into individual wells on a 96-well microtitre plate and incubated overnight at 4 °C. After four rinses with a phosphate-buffered saline with Tween-20 (PBS-T; 80 mM Na_2HPO_4, 1.5 M NaCl, 20 mM KH_2PO_4, 30 mM KCl, 0.5% Tween-20, pH 7.4), the GFP or the TVBMVCP antibody solution was added into each well, and the plate was incubated at 37 °C for 4 hr. After four rinses with the PBS-T an alkaline phosphatase-conjugated goat anti-rabbit IgG solution was added to the wells followed by 4 hr incubation at 37 °C. After the addition of a *p*-nitrophenyl phosphate substrate solution (Sigma, 0.25 mg/ml), the absorbance value (A_{405}) of each well was measured using a microplate reader (BioTek Synergy Mx).

4.7 | Confocal microscopy and fluorescence intensity measurement

To monitor viral intercellular movement and protein subcellular localization in *N. benthamiana* leaves, the agrobacterium-infiltrated leaf patches were collected and examined under a laser confocal microscope (Carl Zeiss). For GFP fluorescence observation, the excitation and emission wavelengths were set at 488 and 520–540 nm, respectively. For DsRed fluorescence observation, the excitation and emission wavelengths were set at 561 and 590–630 nm, respectively. The captured images were processed using the ZEN 2.1 (Carl Zeiss). *Agrobacterium*-infiltrated *N. benthamiana* leaves were photographed under UV light (365 nm) from

a hand-held UV lamp (LUYOR) using a digital camera (Canon 80D). To determine GFP fluorescence intensity in the infiltrated leaf tissues, leaf discs (5 mm in diameter) were sampled from the infiltrated *N. benthamiana* leaf patches with a cork borer and individually placed in wells of a 96-well microtitre plate. GFP fluorescence from each well was determined using a microplate reader (BioTek). The excitation wavelength was 485/10 nm and the emission wavelength was 535/10 nm.

4.8 | Virus particle purification

Virus particles were purified from the infiltrated *N. benthamiana* leaves. At 5 dpai, 15 g of tissues were harvested from the infiltrated leaves, ground in liquid nitrogen, and then homogenized in 30 ml of 0.2 M phosphate buffer at pH 8 and supplemented with 0.15% β-mercaptoethanol and 0.01 M EDTA. The crude extracts were centrifuged at 8,000 × g for 20 min. The supernatant was filtered through four layers of cheesecloth and stirred at 4 °C for 3 hr after adding 1% Triton X-100, 40 g/L polyethylene glycol 6,000, and 0.2 M NaCl. Virus particles were precipitated by centrifugation at 8,000 × g for 20 min, and the pellets were resuspended overnight at 4 °C in a 0.2 M phosphate buffer at pH 8 and containing 1% Triton X-100. Insoluble materials were removed by centrifugation at 8,000 × g for 20 min, and virus particles in the supernatant were pelleted through 1 hr ultracentrifugation at 100,000 × g at 4 °C using an ultracentrifuge CP100WX (Hitachi). The pellets were individually resuspended overnight in a 0.05 M phosphate buffer at pH 8 and at 4 °C. The insoluble materials were removed again by 20 min centrifugation at 8,000 × g. Small amounts of supernatant from each sample were negatively stained with 2% uranyl acetate, loaded onto 230-mesh carbon-coated copper grids, and then examined under a JEM-1200Ex transmission electron microscope (Jeol) for virus particle morphology.

4.9 | Protein expression

Plasmids for expressing the wild-type or mutant CPs were individually transformed into *E. coli* Rosetta cells, and the transformed cells were cultured until OD_{600} = 0.6. The cultures were induced with a 0.1 mM isopropyl-β-D-thiogalactopyranoside solution and incubated at 16 °C for 12 hr. The cultures were pelleted by centrifugation at 8,000 × g for 5 min, and the pellets were individually resuspended with a lysis buffer (50 mM Na_2HPO_4, 300 M NaCl, pH 8.0) followed by 5 min of lysis through sonication on ice. The lysed cells were pelleted by centrifugation at 10,000 × g for 5 min. Supernatants of each sample were transferred into a new clean tube and used as soluble proteins for SDS-PAGE and western blot assays.

ACKNOWLEDGMENTS

We are grateful to Dr Ping Qian from the College of Chemistry and Material Sciences, Shandong Agricultural University, China, and Dr Hong Guo from the University of Tennessee, USA, for their valuable suggestions. This study was supported by the National Natural Science Foundation of China (NSFC; 31720103912), "Taishan Scholar" Construction Project (TS201712023) and funds of the Shandong "Double Tops" Program (SYL2017XTTD11).

DATA AVAILABILITY STATEMENT

The data that support the findings of this study are available from the corresponding author upon reasonable request.

ORCID

Yan-Ping Tian https://orcid.org/0000-0002-3452-2013
Xiang-Dong Li https://orcid.org/0000-0001-9838-0045

REFERENCES

Budyak, I.L., Zhuravleva, A. & Gierasch, L.M. (2013) The role of aromatic-aromatic interactions in strand-strand stabilization of β-sheets. *Journal of Molecular Biology*, 425, 3522–3535.

Butterfield, S.M., Patel, P.R. & Waters, M.L. (2002) Contribution of aromatic interactions to α-helix stability. *Journal of the American Chemical Society*, 124, 9751–9755.

Carrington, J.C., Jensen, P.E. & Schaad, M.C. (1998) Genetic evidence for an essential role for potyvirus CI protein in cell-to-cell movement. *Plant Journal*, 14, 393–400.

Chai, M., Wu, X., Liu, J., Fang, Y., Luan, Y., Cui, X. et al. (2020) P3N-PIPO interacts with P3 via the shared N-terminal domain to recruit viral replication vesicles for cell-to-cell movement. *Journal of Virology*, 94, e01898-19.

Chatterjee, K.S., Tripathi, V. & Das, R. (2019) A conserved and buried edge-to-face aromatic interaction in small ubiquitin-like modifier (SUMO) has a role in SUMO stability and function. *Journal of Biological Chemistry*, 294, 6772–6784.

Cheng, G., Dong, M., Xu, Q., Peng, L., Yang, Z., Wei, T. et al. (2017) Dissecting the molecular mechanism of the sub-cellular localization and cell-to-cell movement of the sugarcane mosaic virus P3N-PIPO. *Scientific Reports*, 7, 9868.

Chung, B.-Y.-W., Miller, W.A., Atkins, J.F. & Firth, A.E. (2008) An overlapping essential gene in the *Potyviridae*. *Proceedings of the National Academy of Sciences of the USA*, 105, 5897–5902.

Crooks, G.E. (2004) WebLogo: a sequence logo generator. *Genome Research*, 14, 1188–1190.

Cui, H. & Wang, A. (2016) Plum pox virus 6K1 protein is required for viral replication and targets the viral replication complex at the early stage of infection. *Journal of Virology*, 90, 5119–5131.

Deng, P., Wu, Z. & Wang, A. (2015) The multifunctional protein CI of potyviruses plays interlinked and distinct roles in viral genome replication and intercellular movement. *Virology Journal*, 12, 141.

Dolja, V.V., Haldeman, R., Robertson, N.L., Dougherty, W.G. & Carrington, J.C. (1994) Distinct functions of capsid protein in assembly and movement of tobacco etch potyvirus in plants. *The EMBO Journal*, 13, 1482–1491.

Dolja, V.V., Haldeman-Cahill, R., Montgomery, A.E., Vandenbosch, K.A. & Carrington, J.C. (1995) Capsid protein determinants involved in cell-to-cell and long distance movement of tobacco etch potyvirus. *Virology*, 206, 1007–1016.

Gao, R., Tian, Y.-P., Wang, J., Yin, X., Li, X.-D. & Valkonen, J.P.T. (2012) Construction of an infectious cDNA clone and gene expression vector of *Tobacco vein banding mosaic virus* (genus *Potyvirus*). *Virus Research*, 169, 276–281.

García, J.A., Glasa, M., Cambra, M. & Candresse, T. (2014) *Plum pox virus* and sharka: a model potyvirus and a major disease. *Molecular Plant Pathology*, 15, 226–241.

Geng, C., Cong, Q.Q., Li, X.D., Mou, A.L., Gao, R., Liu, J.L. et al. (2015) Developmentally regulated plasma membrane protein of *Nicotiana benthamiana* contributes to potyvirus movement and transports to plasmodesmata via the early secretory pathway and the actomyosin system. *Plant Physiology*, 167, 394–410.

Geng, C., Yan, Z.-Y., Cheng, D.-J., Liu, J., Tian, Y.-P., Zhu, C.-X. et al. (2017) Tobacco vein banding mosaic virus 6K2 protein hijacks NbPsbO1 for virus replication. *Scientific Reports*, 7, 43455.

Goldberg, A.L. (2012) Development of proteasome inhibitors as research tools and cancer drugs. *Journal of Cell Biology*, 199, 583–588.

Grangeon, R., Jiang, J., Wan, J., Agbeci, M., Zheng, H. & Laliberté, J.-F. (2013) 6K2-induced vesicles can move cell to cell during turnip mosaic virus infection. *Frontiers in Microbiology*, 4, 351.

Hall, T.A. (1999) BioEdit: a user-friendly biological sequence alignment editor and analysis program for Windows 95/98/NT. *Nucleic Acids Symposium Series*, 41, 95–98.

Huang, C.-H., Foo, M.-H., Raja, J.A.J., Tan, Y.-R., Lin, T.-T., Lin, S.-S. et al. (2020) A conserved helix in the C-terminal region of watermelon silver mottle virus NSs protein is imperative for protein stability affecting self-interaction, RNA silencing suppression, and pathogenicity. *Molecular Plant-Microbe Interactions*, 33, 637–652.

Huang, C.H., Hsiao, W.R., Huang, C.W., Chen, K.C., Lin, S.S., Chen, T.C. et al. (2015) Two novel motifs of watermelon silver mottle virus NSs protein are responsible for RNA silencing suppression and pathogenicity. *PLoS One*, 10, e0126161.

Ivanov, K.I., Puustinen, P., Gabrenaite, R., Vihinen, H., Ronnstrand, L., Valmu, L. et al. (2003) Phosphorylation of the potyvirus capsid protein by protein kinase CK2 and its relevance for virus infection. *The Plant Cell*, 15, 2124–2139.

Ji, S.-X., Wang, S.-W., Wang, J., Li, X.-D., Zhu, T.-S. & Tian, Y.-P. (2018) Preparation and application of antiserum against watermelon mosaic virus coat protein expressed in *E. coli*. *Acta Phytopathologica Sinica*, 48, 833–837.

Jiang, J., Patarroyo, C., Garcia Cabanillas, D., Zheng, H. & Laliberté, J.-F. (2015) The vesicle-forming 6K2 protein of turnip mosaic virus interacts with the COPII coatomer Sec24a for viral systemic infection. *Journal of Virology*, 89, 6695–6710.

Kimalov, B. (2004) Maintenance of coat protein N-terminal net charge and not primary sequence is essential for zucchini yellow mosaic virus systemic infectivity. *Journal of General Virology*, 85, 3421–3430.

Lan, Y.-F., Liu, J.-L., Gao, R., Wang, H.-Y., Zhu, T.-S., Zhu, X.-P. et al. (2007) Expression of tobacco vein banding mosaic virus coat protein in *E. coli* and preparation of antiserum. *Acta Phytopathologica Sinica*, 37, 461–466.

Liu, H.T. & Naismith, J.H. (2008) An efficient one-step site-directed deletion, insertion, single and multiple-site plasmid mutagenesis protocol. *BMC Biotechnology*, 8, 91.

Lõhmus, A., Hafrén, A. & Mäkinen, K. (2017) Coat protein regulation by CK2, CPIP, HSP70, and CHIP is required for potato virus A replication and coat protein accumulation. *Journal of Virology*, 91, e01316–e1416.

Movahed, N., Patarroyo, C., Sun, J., Vali, H., Laliberté, J.-F. & Zheng, H. (2017) Cylindrical inclusion protein of turnip mosaic virus serves as a docking point for the intercellular movement of viral replication vesicles. *Plant Physiology*, 175, 1732–1744.

O'Leary, N.A., Wright, M.W., Brister, J.R., Ciufo, S., Haddad, D., McVeigh, R. et al. (2016) Reference sequence (RefSeq) database at NCBI: current status, taxonomic expansion, and functional annotation. *Nucleic Acids Research*, 44, D733–D745.

Olspert, A., Chung, B.-Y.-W., Atkins, J.F., Carr, J.P. & Firth, A.E. (2015) Transcriptional slippage in the positive-sense RNA virus family *Potyviridae*. *EMBO Reports*, 16, 995–1004.

Olzmann, J.A., Brown, K., Wilkinson, K.D., Rees, H.D., Huai, Q., Ke, H. et al. (2004) Familial Parkinson's disease-associated L166P mutation disrupts DJ-1 protein folding and function. *Journal of Biological Chemistry*, 279, 8506–8515.

Olzmann, J.A., Li, A., Chudaev, M.V., Chen, J., Perez, F.A., Palmiter, R.D. et al. (2007) Parkin-mediated K63-linked polyubiquitination targets misfolded DJ-1 to aggresomes via binding to HDAC6. *Journal of Cell Biology*, 178, 1025–1038.

Rege, N.K., Wickramasinghe, N.P., Tustan, A.N., Phillips, N.F.B., Yee, V.C., Ismail-Beigi, F. et al. (2018) Structure-based stabilization of insulin as a therapeutic protein assembly via enhanced aromatic–aromatic interactions. *Journal of Biological Chemistry*, 293, 10895–10910.

Revers, F. & García, J.A. (2015) Molecular biology of potyviruses. In: Maramorosch, K. & Mettenleiter, T.C. (Eds.) *Advances in Virus Research*. Cambridge, MA: Academic Press, pp. 101–199.

Ritzenthaler, C. (2011) Parallels and distinctions in the direct cell-to-cell spread of the plant and animal viruses. *Current Opinion in Virology*, 1, 403–409.

Roberts, I.M., Wang, D., Findlay, K. & Maule, A.J. (1998) Ultrastructural and temporal observations of the potyvirus cylindrical inclusions (CIs) show that the CI protein acts transiently in aiding virus movement. *Virology*, 245, 173–181.

Rodamilans, B., Valli, A., Mingot, A., San León, D., Baulcombe, D., López-Moya, J.J. et al. (2015) RNA polymerase slippage as a mechanism for the production of frameshift gene products in plant viruses of the *Potyviridae* family. *Journal of Virology*, 89, 6965–6967.

Rodríguez-Cerezo, E., Findlay, K., Shaw, J.G., Lomonossoff, G.P., Qiu, S.G., Linstead, P. et al. (1997) The coat and gylindrical inclusion proteins of a potyvirus are associated with connections between plant cells. *Virology*, 236, 296–306.

Schoelz, J.E., Harries, P.A. & Nelson, R.S. (2011) Intracellular transport of plant viruses: finding the door out of the cell. *Molecular Plant*, 4, 813–831.

Scholthof, K.B.G., Adkins, S., Czosnek, H., Palukaitis, P., Jacquot, E., Hohn, T. et al. (2011) Top 10 plant viruses in molecular plant pathology. *Molecular Plant Pathology*, 12, 938–954.

Seglen, P.O. & Gordon, P.B. (1982) 3-Methyladenine: specific inhibitor of autophagic/lysosomal protein degradation in isolated rat hepatocytes. *Proceedings of the National Academy of Sciences of the USA*, 79, 1889–1892.

Seo, J.K., Vo Phan, M.S., Kang, S.H., Choi, H.S. & Kim, K.H. (2013) The charged residues in the surface-exposed C-terminus of the soybean mosaic virus coat protein are critical for cell-to-cell movement. *Virology*, 446, 95–101.

Shukla, D.D., Strike, P.M., Tracy, S.L., Gough, K.H. & Ward, C.W. (1988) The N and C termini of the coat proteins of potyviruses are surface-located and the N terminus contains the major virus-specific epitopes. *Journal of General Virology*, 69, 1497–1508.

Tatineni, S., Kovacs, F. & French, R. (2014) Wheat streak mosaic virus infects systemically despite extensive coat protein deletions: identification of virion assembly and cell-to-cell movement determinants. *Journal of Virology*, 88, 1366–1380.

Tavert-Roudet, G., Anne, A., Barra, A., Chovin, A., Demaille, C. & Michon, T. (2017) The potyvirus particle recruits the plant translation initiation factor eIF4E by means of the VPg covalently linked to the viral RNA. *Molecular Plant-Microbe Interactions*, 30, 754–762.

Valkonen, J.P.T. (2007) Viruses: economical losses and biotechnological potential. In: Vreugdenhil, D., Bradshaw, J., Gebhardt, C., Govers, F., Mackerron, D.K.L., Taylor, M.A. & Ross, H.A. (Eds.) *Potato Biology and Biotechnology*. Amsterdam: Elsevier, pp. 619–641.

Wei, T.Y., Zhang, C.W., Hong, J., Xiong, R.Y., Kasschau, K.D., Zhou, X.P. et al. (2010) Formation of complexes at plasmodesmata for potyvirus intercellular movement is mediated by the viral protein P3N-PIPO. *PLoS Pathogens*, 6, e1000962.

Wylie, S.J., Adams, M., Chalam, C., Kreuze, J., Jose López-Moya, J., Ohshima, K. et al. (2018) ICTV virus taxonomy profile: *Potyviridae*. *Journal of General Virology*, 98, 352–354.

Xu, Y., Silva, W.L.D., Qian, Y. & Gray, S.M. (2018) An aromatic amino acid and associated helix in the C-terminus of the potato leafroll virus minor capsid protein regulate systemic infection and symptom expression. *PLoS Pathogens*, 14, e1007451.

SUPPORTING INFORMATION

Additional supporting information may be found online in the Supporting Information section.

How to cite this article: Yan Z-Y, Cheng D-J, Liu L-Z, et al. The conserved aromatic residue W^{122} is a determinant of potyviral coat protein stability, replication, and cell-to-cell movement in plants. *Mol Plant Pathol*. 2021;22:189–203. https://doi.org/10.1111/mpp.13017